Energy 189 (2019) 116199

Contents lists available at ScienceDirect

Energy

journal homepage: www.elsevier.com/locate/energy

Energy-harvesting variable/constant damping suspension system with motor based electromagnetic damper

Shiying Li [a, b], Jun Xu [a, b, *], Xiaohui Pu [a, b], Tao Tao [a, b], Haonan Gao [a, b], Xuesong Mei [a, b]

[a] State Key Laboratory for Manufacturing Systems Engineering, Xi'an Jiaotong University, Xi'an, Shaanxi, 710049, China
[b] Shaanxi Key Laboratory of Intelligent Robots, School of Mechanical Engineering, Xi'an Jiaotong University, Xi'an, Shaanxi, 710049, China

ARTICLE INFO

Article history:
Received 9 April 2019
Received in revised form
11 September 2019
Accepted 23 September 2019
Available online 25 September 2019

Keywords:
Energy-harvesting
Variable damping
Regenerative suspension
Adjustable damping
Electromagnetic damper
Vibration energy recovery

ABSTRACT

Energy-harvesting suspension is very important to improve the energy efficiency of vehicles, especially for electric vehicles. A novel energy-harvesting variable/constant damping suspension system with motor based electromagnetic damper is proposed in this paper. The method attempts to make following contributions: The vehicle vibration energy is not only harvested from the suspension system, but also controlled to store in the battery for further usage. Moreover, the damping of the suspension system is able to be controlled as wish, to be constant or to vary with road conditions. The performance comparison with conventional suspension equipped with an oil damper is carried out by simulation and experiments. The effect of the moment of inertia on the suspension performance is investigated. To experimentally validate the proposed method, a scaled quarter car suspension validation platform is established. The experimental results show that the damping can be controlled to be constant as the conventional oil damper, and also be variable as wish. The proposed energy-harvesting suspension can recover energy from vehicle vibration to store in the battery for further usage with high efficiency, which is as high as 35.24% improvement compared with previous studies. Meanwhile, the damping coefficient can also be regulated in real-time accurately.

1. Introduction

As one of the most promising solutions to the oil crisis and environmental problems, electric vehicles (EVs) are becoming more and more important and popular [1]. However, for the limitation of battery technologies, the drive distance is considered as one of the main factors hindering the market penetration of EVs. On the one hand, the energy stored in the batteries should be efficiently utilized, which have been studied in many researches, such as obtaining accuracy states of the battery [2], hybridizing with supercapacitors [3], battery string balancing [4] and reconfiguration [5], etc. On the other hand, more other energy should be produced, or so-called regenerative technology. The traction motor braking energy regeneration has been widely studied [6] and becomes more and more mature [7]. Similarly, another regenerative technology, the regenerative suspension system, draws more and more attentions [8]. As shown in Ref. [9], only 12%–30% of the fuel energy is used to overcome the resistance from road friction and air drag, and one major loss is vibration dissipation in the shock absorber. As demonstrated by Zuo [10] and Zhang [11], 100W–400W average power is available in the suspension at 60 km/h on B and C class road for a middle-sized vehicle. If this energy is harvested, the fuel efficiency can be improved by 20% [12].

The traditional passive suspension system is widely used for the standard performance: simple, reliable, and cost-effective. But, limited by the immutable damping coefficient, the damping force can't be regulated to suppress the unpredictable disturbances to vehicle body adaptively [13]. In addition, the severe temperature-rise of damping oil will lead to attenuation of the damping force and acceleration of the suspension system failure [14]. An electromagnetic damper (EMD) can overcome these shortcomings because the damping coefficient can be regulated by the power circuit in real-time, and the absorbed energy by the damper can be harvested and stored.

The EMD is the key component to realize both the energy harvest and the damping control functions for an energy-harvesting suspension. The EMD can be divided into the linear machine type and the rotary machine type, according to the generator type. The

* Corresponding author. State Key Laboratory for Manufacturing Systems Engineering, Xi'an Jiaotong University, Xi'an, Shaanxi, 710049, China.
E-mail address: xujunx@xjtu.edu.cn (J. Xu).

https://doi.org/10.1016/j.energy.2019.116199
0360-5442/

Nomenclature

P_{in}	input power of a damper (W)
P_{out}	output power of a damper (W)
C	damping coefficient (Ns/m)
v	vibration speed (m/s)
η	efficiency of DC/DC (%)
m_s	sprung mass (kg)
m_u	unsprung mass (kg)
k_1	suspension stiffness (N/m)
k_2	tire stiffness (N/m)
x_s	displacement of sprung mass (m)
x_u	displacement of unsprung mass (m)
x_g	displacement of ground (m)
b	inerter mass (kg)
c_{eq}	equivalent damping coefficient (Ns/m)
c_{eq_ref}	reference damping coefficient (Ns/m)
c_{eq_act}	actual damping coefficient (Ns/m)
F	damping force (N)
J	moments of inertia of damper (kg m^2)
J_M	moment of inertia of motor rotor (kg m^2)
J_S	moment of inertia of screw-rod (kg m^2)
c_{em_ref}	reference rotary damping coefficient (Ns/m)
c_{em_act}	actual rotary damping coefficient (Ns/m)
l	lead of ball-screw (m)
T_e	motor torque (Nm)
T_{e_ref}	reference motor torque (Nm)
ω	motor speed (rad/s)
Ω	motor speed (r/min)

Abbreviation

EV	Electric Vehicle
PMSM	Permanent Magnet Synchronous Motor
EMD	Electromagnetic Damper
BA	vehicle Body Acceleration
DTD	Dynamic Tire Deformation
SWS	Suspension Workspace State
U_L	voltage of load (V)
R_L	resistance of load (Ω)
e_a, e_b, e_c	stator voltage of a PMSM (V)
r_s	stator resistance of a PMSM (Ω)
L_s	stator inductance of a PMSM (H)
E	peak value of induced electromotive force (V)
i_L	load current (A)
θ	rotor electric angle (rad)
K_e	Back-EMF coefficient of a PMSM (Vs/rad)
α	duty cycle of PWM signals
i_A, i_B, i_C	phase-current of a PMSM (A)
i_{q_act}, i_{d_act}	d and q current of a PMSM (A)
ψ_f	rotor flux of a PMSM (VRad^{-1})
P	pole pairs of a PMSM
T_{ref}, T_{act}	reference and actual motor torque (Nm)
ΔW	mechanical input work (J)
A	amplitude of sine excitation (m)
$\eta_{DC/DC}$	efficiency of the DC/DC converter
η_{sys}	energy-harvesting efficiency of system
P_{in_ave}	average input power of system (W)
P_{out_ave}	average recovery power of system (W)
i_{bat}	battery pack current (W)
u_{bat}	battery pack voltage (W)
n_0	the reference spatial frequency (0.1 m^{-1})
G_{x_g}	power spectrum density of road excitation
u	vehicle velocity
BLDC	Brushless DC electric motor
CCM	Continuous Conduction Mode
DCM	Discontinuous conduction mode
2DOF	Two Degree of Freedom
PSD	Power Spectrum Density

linear type EMD can translate the reciprocating motion of vibration to motion of cutting the magnetic inductions lines directly and is characterized by a simple structure and same dynamic character with a conventional oil damper. In the early 1980s, Karnopp first verified the feasibility of harvesting energy and adjusting damping by a linear permanent machine and an adjustable resistor. However, since not all the magnets contribute the force in the linear motor, the power density was low, and the size was often big [15]. How to improve power density and get an effective damping coefficient is a major research direction [16]. Babak Ebrahimi utilized the eddy current damping effect as a damping source and regulated the extra load to change the electromagnetic damping force [17]. By these ways, the total weight could be reduced by 53% while a 1570 N/m passive damping was achieved, but the energy dissipated by eddy current loss can't be harvested successfully. Asadi Ehasn combined a hydraulic damper and linear electromagnetic damper together in a single cylinder to get a hybrid damper, thus it can supply a bigger and more reliable damping force from 1302 to 1540 N/m [18]. However, the hydraulic component also dissipated the energy into the air in the heat form and decreased the recovery efficiency dramatically.

For the rotary type EMD, a linear-to-rotary movement conversion mechanism is needed to convert the reciprocating motion of vibration to rotary motion of the motor [19], such as ball-screw [20], gear and rack [21], hydraulic cylinder and pump [22] and some other mechanisms [23]. Compared with the linear type EMD, the structure of a rotary type EMD is more complex due to the movement conversion mechanism, but the power density can be bigger. Whereas, there is also a shortcoming that dynamic characteristics of the suspension are changed as a result of the introduced moment of inertia that mainly consists of the movement conversion mechanism and motor rotor. As demonstrated by L. Pires that the linear-to-rotational EMD can be modeled as an inerter in parallel with a conventional oil damper [24]. How the moment of inertia affects dynamic performances of the suspension need to be further studied before it is employed on a vehicle.

The EMD converts the kinetic energy to electricity, and the power circuit is used to regulate motor current to act as a variable load and to get a controllable damping coefficient. In the previous studies, the resistance load was mostly used as the load, and the damping coefficient can be changed by regulating the resistance [25]. To regulate the damping in real-time, a Mosfet was connected to a resistor in parallel by Donghong Ning [26], and the equivalent resistance can be regulated through regulating the duty cycle of the PWM signals that drive the Mosfet. In such methods, the regenerated energy was dissipated in the resistance load, and no energy was stored for further usage, which was not applicable in real implementations.

On the other hand, batteries were used directly to store the regenerated energy. However, with the direct battery load, the damping failure zone is inevitable in proportion to the battery voltage: when the induced voltage of the generator in the EMD is lower than the battery voltage, there is no current through the motor, and no damping is generated. To overcome this

shortcoming, Chen [27] and Yohji [28] regulated the number of batteries to regulate the output voltage, and to get a controllable damping force, but the minimum damping was limited by the battery voltage and resistance. Zutao Zhang [29] and Waleed Salman [21] employed a voltage regulator LM117 to get a steady output current to charge the battery, and obtained an average recovery efficiency of 40% and 44.24% respectively. Ruochen Wang [30] used a boost topology DC/DC converter to keep a steady output voltage to charge the battery, and a 20.1% recovery efficiency was obtained. However, steady output voltage results in a steady output power P_{out} if the change of open circuit voltage (OCV) of the battery pack is neglected in a short time period. According to the relationship between damping coefficient c, vibration speed v and input vibration power P_{in}, $P_{in}=cv^2$, the system input power varies with the vibration speed v. Based on the law of the convention of energy, $P_{out} = P_{in}\cdot\eta$, the damping coefficient c varies with the transfer efficiency η and vibration speed v: the higher the transferring efficient η and the lower the speed v, the bigger the damping coefficient c.

The previous studies concentrate mostly on the energy recovering, and seldom pay much attention to the influence of the variable damping coefficient on the suspension system dynamic. How to design and realize an energy-harvesting system taking into account the influence of the power circuit response and moment of inertia composed from the motor rotor and transmission on the dynamic performance, has not been given a solution in previous studies.

As analyzed above, although there are already many studies on energy harvesting suspension and energy harvesting shock absorber, some challenges remain: (1) the EMD is studied a lot, whereas seldom pay much attention to the electromagnetic suspension system design; (2) The influence of introduced moment of inertia of a rotary style EMD need to be further studied before the electromagnetic suspension is applied to a real car. (3) How to realize energy harvest and damping control in real-time, rather than dissipate the vibration energy into the air with a resistance need to be addressed. To address these shortcomings, this paper aims at designing and realizing an energy-harvesting suspension that considering the damping control comprehensively in real-time, energy recovery and energy store, vehicle dynamic performance. The main contributions of this paper are as follows:

(1) A ball-screw based EMD employing a PMSM as the generator is designed, with the power circuit and control method, the EMD damping can be adjusted in real-time, and the vibration energy can be harvested and stored.
(2) The energy-harvesting vehicle dynamical model (2DOF) is modeled, and the dynamic performances are studied and verified by simulation and experiments, compared with a conventional suspension equipped with an oil damper.
(3) This paper gives a realization solution of the energy-harvesting suspension from the system level, considering the whole suspension system including damping control, energy harvest and system analysis, which gives guidance for the following design and study of energy-harvesting suspension.

This paper is organized as follows. The design principle of an energy-harvesting suspension and control circuits for the energy-harvesting device is introduced in Section 2. The energy-harvesting vehicle dynamical model (2DOF) is built, and how the moment of inertia caused by the motor rotor and transmission affects the performance of a suspension is analyzed in Section 3. In Section 4, experiment details and experiment results for the variation of the proposed energy-harvesting system are presented. Finally, the conclusions are summarized in Section 5.

2. Design of energy-harvesting suspension system

2.1. Overview of an energy-harvesting suspension system

A typical energy-harvesting suspension equipped with a motor-ball-screw based EMD is shown in Fig. 1. Besides the mounting part and connecting parts, the EMD architecture mainly consists of a motor and a ball-screw. The ball-screw is used to convert the oscillation between the vehicle body and the chassis to the rotary motion of the motor. The electric motor works as a generator to convert the kinetic energy of the suspension into electricity. The power circuit is a voltage or current regulator which can convert the AC current generated by the generator into steady DC current to charge the battery.

Because of the impact of the moment of inertia composed by the motor shaft and the screw-rod, the EMD can be regarded as a conventional oil damper connected by an inerter in parallel [31] as shown in Fig. 1. The total damping force F of the damper can be given by

$$F = b(\ddot{x}_u - \ddot{x}_s) + c_{eq}(\dot{x}_u - \dot{x}_s) \tag{1}$$

where x_u, x_s are the displacements of the sprung mass and unsprung mass respectively, c_{eq} is equivalent damping coefficient of the EMD, and the inerter value b is expressed by

$$b = J\frac{4\pi^2}{l^2} \tag{2}$$

where J is the sum of moments of inertia of the EMD, which mainly consists of the moment of inertia of the motor rotor J_M and screw-rod J_S. Assume the rotary damping coefficient of the motor is c_{em}, the linear equivalent damping coefficient c_{eq} is expressed by

$$c_{eq} = c_{em}\left(\frac{2\pi}{l}\right)^2 \tag{3}$$

where l is the lead of the ball-screw and it is a constant value. Thus, the linear damping coefficient c_{eq} can be regulated by regulating the motor rotary electromagnetic damping c_{em} directly.

2.2. Analysis of rotary damping coefficient

With a typical resistive load, a damper power circuit is shown in

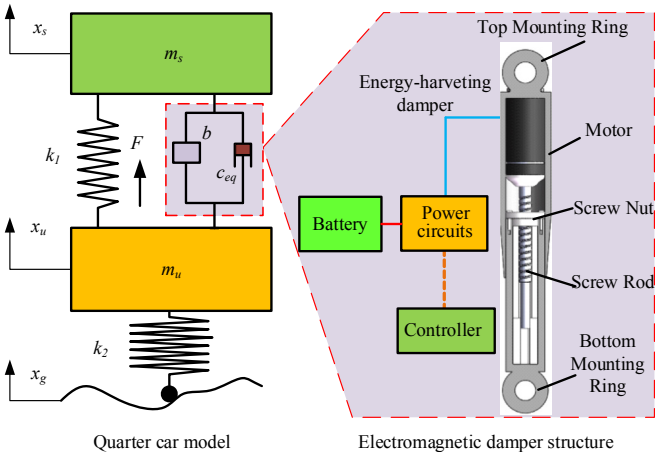

Fig. 1. Quarter car model equipped with an EMD.

Fig. 2, where a permanent magnet synchronization motor (PMSM) is employed to be a generator. For a PMSM, the rotary damping coefficient c_{em} is defined by

$$c_{em} = T_e/\omega \tag{4}$$

where T_e is the motor torque and ω is speed. However, the torque can't get directly, because the d-axis i_d and q-axis i_q current are necessary to estimate the torque. Based on the law of energy conservation, we can get the torque calculation formula indirectly.

Ignoring the effect of commutation of the armature current and assuming that only two phases are connected to the circuit and contribute to the torque at any moment, the output current i_L can be expressed by

$$i_L = \frac{\sqrt{3}E\sin\left(p\omega t + \frac{\pi}{3} - k\frac{\pi}{3}\right)}{2r_s + R_L}; \quad p\omega t \in \left[k\frac{\pi}{3}, (k+1)\frac{\pi}{3}\right], \quad k = 0, 1, 2, 3\ldots \tag{5}$$

where p is the pole pairs of the PMSM, and r_s is the inner resistance of the stator coil. E is the peak value of induced electromotive force (e_a, e_b, e_c), and it is determined by $E = K_e\omega$, in which K_e is the Back-EMF coefficient. According to the energy transformations relations, the generated electricity is all converted into thermal energy that dissipated on the resistance.

$$T_e\omega = i_L^2(2r_s + R_L) \tag{6}$$

Then, the rotary damping coefficient can be obtained by

$$c_{em} = \frac{3K_e^2\sin^2\left(\theta + \frac{\pi}{3} - k\frac{\pi}{3}\right)}{2r_s + R_L}, \theta \in \left[k\frac{\pi}{3}, (k+1)\frac{\pi}{3}\right], k = 0, 1, 2, 3\cdots \tag{7}$$

where $\theta = p\omega t$ is the rotor position. Obviously, the damping coefficient value varies with the rotor position θ.

Taking into account the torque ripple caused by the commutation lag, Eq. (7) can be modified as follow:

$$c_{em} = \frac{3K_e^2\sin^2\left(\theta + \frac{\pi}{3} - k\frac{\pi}{3}\right)}{2r_s + R_L} + \Delta c_{em}, \theta \in \left[k\frac{\pi}{3}, (k+1)\frac{\pi}{3}\right], k = 0, 1, 2, 3\cdots \tag{8}$$

where Δc_{em} is caused by the torque ripple, and it varies with the speed and current [32].

It can be seen from Eq. (8) that: (1) The damping coefficient changes with the rotor position with the resistive load; (2) As a result of computation, the torque ripple leads to damping coefficient uncertainty, this consequence occurs for a BLDC consideration as well; (3) The damping coefficient can be regulated by changing the load, and when the resistance is 0 or stator terminals are shorted, the damping coefficient reaches the maximum.

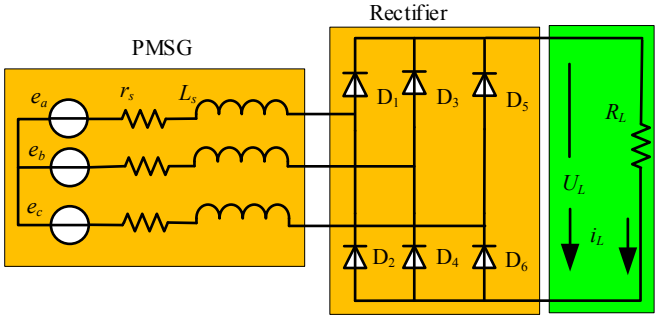

Fig. 2. Power circuit with a resistive load.

2.3. Design of a damping-variable energy-harvesting suspension

With the above-mentioned topology in Fig. 2, the energy generated by the EMD is dissipated by the resistor R_L and r_s, besides, the damping coefficient varies all the time with the rotor position. To deal with these problems, following energy-harvesting variable/constant damping suspension system is proposed as shown in Fig. 3.

A surface mounted PMSM is employed to convert the vibration energy to electricity. Then, the three-phase AC current is converted to DC current by the rectifier and filter. A DC/DC converter with the capacity of boosting and reducing the output voltage is utilized to regulating the output current or voltage to charge the battery, acting as a variable load for the generator. Through regulating the duty α of the PWM pulse based on the reference damping coefficient c_{eq_req} from the VCU (Vehicle control unit), the output current of the DC/DC converter can be controlled by the control unit, so does the damping torque T_e and damping coefficient c_{eq_act}. The DC/DC converter and control unit are the key components in the power circuit, and they are introduced detailly in the following sections.

2.3.1. DC/DC converter unit

A buck-boost topology is selected to be the DC/DC converter in our design, as shown in Fig. 4. There are two different operating modes for a buck-boost converter: (1) discontinuous conduction mode (DCM), (2) continuous conduction mode (CCM) [33]. When the buck-boost converter works in DCM, the output voltage is related to both the load and PWM period T, and it is expressed by

$$U_{out} = \frac{P_{in}}{i_{out}}\eta = \frac{U_{in}^2 T\alpha^2}{2L_f i_{\text{out}}}\eta \tag{9}$$

where the η is the efficiency of the converter, and it varies with the input and output power. α is the duty of the PWM pulse. L is the inductance of the inductor. When the buck-boost converter works in CCM, the output voltage is expressed by :

$$U_{out} = \frac{U_{in}\alpha}{1-\alpha} \tag{10}$$

So, the output voltage can be regulated by adjusting the PWM duty cycle α in both CCM and DCM.

2.3.2. PMSM and control units

The control unit can be a controller equipped with the basic ADC module, QEP (quadrature encoder pulse) module, and PWM module. The ADC module is used to get the three-phase currents (i_A, i_B, i_C), and the QEP module is used to decode the quadrature encoder pulse signals from the encoder to obtain the motor speed ω and rotor position θ. According to Eq. (3) the preset damping coefficient c_{eq_ref} from the VCU can be obtained by controlling the rotary damping coefficient c_{em_ref}. The actual damping coefficient c_{em_act} can be obtained by

$$c_{em\_act} = \frac{T_{e\_act}}{\omega} \tag{11}$$

where T_{e_act} is the actual torque of the motor. If we regulate the damping coefficient using a PI controller directly, there is a big calculation error as a result of the division in Eq. (11), because the

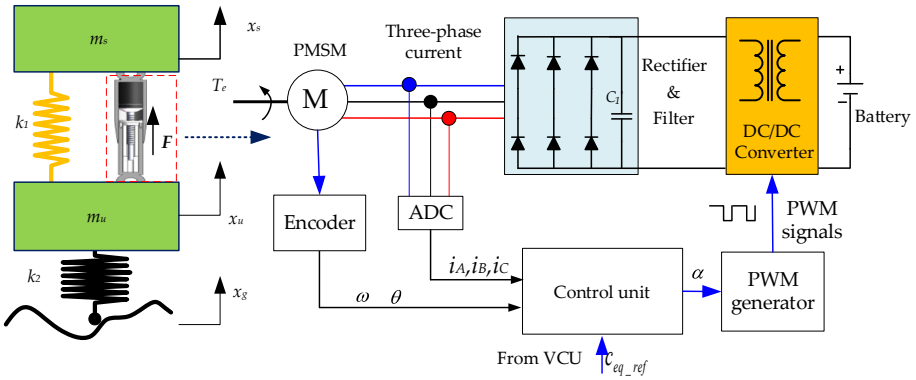

Fig. 3. The energy-harvesting variable/constant damping suspension system.

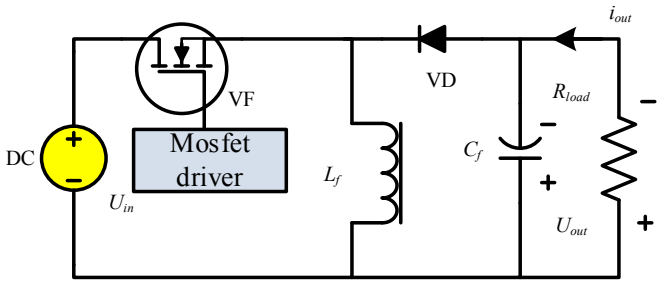

Fig. 4. The buck-boost converter topology.

speed ω can be zero. Therefore, we can replace the damping coefficient regulation with torque regulation: regulate the output power to regulate the motor torque to let the actual torque T_{e_act} track the reference torque T_{e_ref}, and the aim of regulating the damping can be obtained indirectly.

The actual torque T_{e_act} of the surface mounted PMSM can be obtained by

$$T_{e\_act} = \frac{3}{2} p \psi_f i_{q\_act} \tag{12}$$

where the ψ_f is the rotor flux, and actual q-axis current i_{q_act} is obtained by Clarke and Park transforms from the three-phase current of i_A, i_B, i_C:

$$i_{q\_act} = \frac{2}{3}\left[- i_A \sin(\theta) - i_B \sin\left(\theta - \frac{2}{3}\pi\right) - i_C \sin\left(\theta + \frac{2}{3}\pi\right)\right] \tag{13}$$

Given the rotor speed ω and preset rotary damping coefficient c_{em}, the required torque T_{e_ref} is obtained by

$$T_{e\_ref} = \omega c_{em\_ref} \tag{14}$$

Because the required torque T_{e_ref} varies with speed ω all the time, the control system must be characterized with a high response speed to make sure that the actual torque T_{e_act} can track the required torque T_{e_ref} well. There are two solutions: (1) increase the regulate frequency of the control unit; (2) increase the response speed of the buck-boost converter by reducing the inductance L_f and PWM period T.

Based on the analysis above, the system logic control block is given in Fig. 5.

It should be noted that the torque tracking error is given by $\left|T_{e\_ref}\right| - \left|T_{e\_act}\right|$ rather than $T_{e\_ref} - T_{e\_act}$ in Fig. 5. This is because the buck-boost converter can only regulate the magnitude of the damping torque but can't regulate the direction of the torque as a result of the rectifier. In addition, when the required value T_{e_ref} and actual value T_{e_act} are opposite as a result of measurement error, the tracking error will be greater instead of converging to zero. But this case only comes up when the vibration is weak, and the current is very small, which does not last for long.

The error of the absolute torque is sent to a PI controller, and a PWM duty cycle α is obtained. Through a PWM generator, a PWM signal characterized with the duty cycle α is generated to drive the MOSFET in the DC/DC converter to regulate the input and output current to get the desired damping torque T_{e_ref}.

3. Modeling and analysis

Due to the effect of inerter, the energy-harvesting suspension system dynamic is different from a conventional one according to (1). To study the effect of the inerter on the suspension, a car model is introduced in Table 1. The inerter mass is calculated based on a prototype that is introduced in Section 4, which consists of a PMSM with a moment of inertia of 4.73×10^{-5} kgm^2 and a ball screw characterized with a lead of 0.016 m and a moment of inertia of 1.20×10^{-6} kgm^2.

3.1. Effect of additional inerter on the inherent frequency of the suspension

The inherent frequency of a suspension is a very important parameter to evaluate the ride comfort, and the vertical vibration frequency that the human body is used to is about 1–1.6hz.

For a quarter car suspension model employed in Fig. 1, the m_s and m_u stands for the sprung mass and unsprung mass respectively; x_s and x_u are the displacement of the sprung mass and unsprung mass respectively; x_g represents the road excitation; k_1 and k_2 are suspension stiffness and tire respectively, the tire damping is neglected.

Based on Newton's second law, the system differential equation can be obtained as follow:

$$m_s \ddot{x}_s = k_1(x_u - x_s) + c_{eq}(\dot{x}_u - \dot{x}_s) + b(\ddot{x}_u - \ddot{x}_s) \tag{15}$$

$$m_u \ddot{x}_u = -k_1(x_u - x_s) - c_{eq}(\dot{x}_u - \dot{x}_s) - b(\ddot{x}_u - \ddot{x}_s) + k_2(x_g - x_u) \tag{16}$$

For a conventional suspension equipped with an oil damper, there is no inerter component or $b = 0$. Rearrange the differential

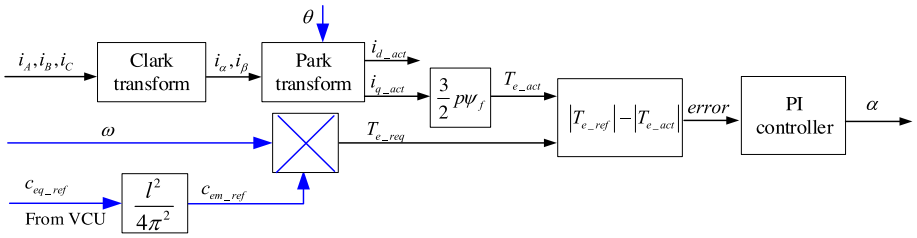

Fig. 5. System logic control block.

Table 1
Parameters of a quarter car model.

Suspension parameters		Value
Conventional Suspension with oil damper	Sprung mass (m_s/kg)	317.5
	Unsprung mass (m_u/kg)	32.5
	Damping coefficient (c_s/Nsm^{-1})	1500
	Spring stiffness (k_1/Nm^{-1})	22000
	Tire stiffness (k_2/Nm^{-1})	192000
Energy-harvesting suspension with EMD	Inerter mass (b/kg)	7.48
	Lead of the ball-screw (l/m)	0.016
	Moment of inertia of motor rotor (J_M/kgm^2)	4.73×10^{-5}
	Moment of inertia of screw rod (J_S/kgm^2)	1.20×10^{-6}

equation (15) and equation (16) as follow:

$$[(1+\lambda_u)m_s + b]\ddot{x}_s = k_1(x_u - x_s) + c_{eq}(\dot{x}_u - \dot{x}_s) + \lambda_u k_2(x_g - x_u) \tag{17}$$

$$[(1+\lambda_s)m_u + b]\ddot{x}_u = -k_1(x_u - x_s) - c_{eq}(\dot{x}_u - \dot{x}_s) + (1+\lambda_s)k_2(x_g - x_u) \tag{18}$$

where $\lambda_u = b/m_u$, $\lambda_s = b/m_s$. The non-damping free vibration equations are

$$\mathbf{M}\ddot{\mathbf{x}} + \mathbf{K}\mathbf{s} = \mathbf{0} \tag{19}$$

where $\mathbf{M} = \begin{bmatrix} (1+\lambda_u)m_s + b & 0 \\ 0 & (1+\lambda_s)m_u + b \end{bmatrix} \mathbf{K} = \begin{bmatrix} k_1 & -k_1 + \lambda_u k_2 \\ -k_1 & k_1 + (1+\lambda_s)k_2 \end{bmatrix}$.

Thus, the characteristic equations of the undamped linear system are

$$\left|\mathbf{K} - \omega^2\mathbf{M}\right| = 0 \tag{20}$$

and the roots of the characteristic equation are

$$\omega_{1,2}^2 = \frac{1}{2}(a+d) \mp \frac{1}{2}\sqrt{(a+d)^2 - 4(ad-bc)} \tag{21}$$

where $a = \frac{k_1 m_u}{m}$, $b = \frac{k_1 m_u - k_2 b}{m}$, $c = \frac{k_1 m_s}{m}$, $d = \frac{k_1 m_s + k_2(m_s+b)}{m}$, $m = m_s m_u + m_s b + m_u b$.

The lower value and higher value of the roots are first-order and second-order natural frequency, respectively. Substitute the parameters in Table 1 into the roots of the characteristic (21), the system natural frequency changing curves with the inerter are plotted in Fig. 6.

From Fig. 6, we can see that both first-order and second-order natural frequency reduces with the increase of the inerter mass. It means a conventional suspension system if $b = 0$ and an energy-harvesting suspension system if $b = 4\pi^2 J/l^2$. The first order and second-order natural frequencies of the suspension system with no inerter are 1.255 Hz and 12.93 Hz respectively, and those of a suspension system with an EMD are 1.243 Hz and 11.66 Hz, declining 0.96% and 9.82% respectively. Considering the excitation frequency from the road can hardly get more than 10 Hz, the effect of inerter with the parameter in Table 1 on the suspension performance is very small. But, if the inerter mass b gets three times of given value $b = 24\pi J/l^2$, the second-order natural frequency gets less than 10 Hz, and the effect can't be neglected.

3.2. Effect of additional inerter on transmission characteristics of the suspension in sine excitation

There are three performance indexes for suspension evaluation: (1) vehicle body acceleration ($BA = \ddot{x}_s$) which represents the ride comfort; (2) dynamic tire deformation ($DTD = x_g - x_u$) which represents the handling stability; (3) the suspension workspace state ($SWS = x_u - x_s$) which is limited by the largest stroke of the damper. Thus, these three performance indexes are selected to be the study objects affected by the moment of inerter.

Rearranging equations (14) and (15), the matrix form of the dynamic equation can be expressed as:

$$\dot{\mathbf{x}} = \mathbf{A}\mathbf{x} + \mathbf{F}x_g \tag{22}$$

where $x = [x_s, \dot{x}_s, x_u, \dot{x}_u]^T$ and

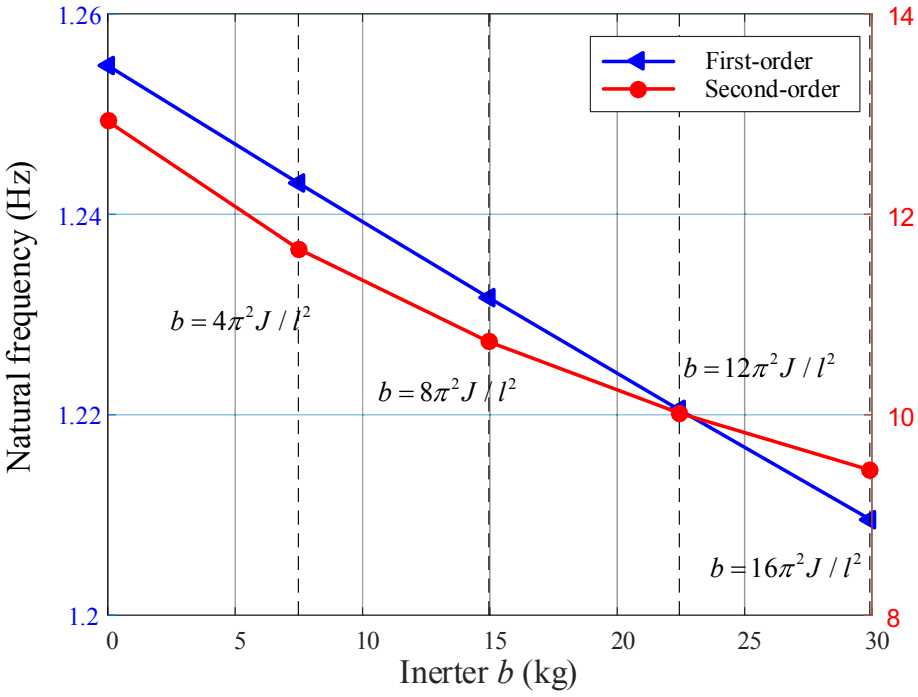

Fig. 6. The system natural frequency changes with the equivalent inertia mass.

$$\mathbf{A}=\begin{bmatrix} 0 & 1 & 0 & 0 \\ \frac{-k_1}{(1+\lambda_u)m_s+b} & \frac{-c_{eq}}{(1+\lambda_u)m_s+b} & \frac{k_1-\lambda_u k_2}{(1+\lambda_u)m_s+b} & \frac{c_{eq}}{(1+\lambda_u)m_s+b} \\ 0 & 0 & 0 & 1 \\ \frac{k_1}{(1+\lambda_s)m_u+b} & \frac{c_{eq}}{(1+\lambda_s)m_u+b} & \frac{-k_1-(1+\lambda_s)k_2}{(1+\lambda_s)m_u+b} & \frac{-c_{eq}}{(1+\lambda_s)m_u+b} \end{bmatrix}$$

$$\mathbf{F}=\begin{bmatrix} 0 \\ \frac{\lambda_u k_2}{(1+\lambda_u)m_s+b} \\ 0 \\ \frac{(1+\lambda_s)k_2}{(1+\lambda_s)m_u+b} \end{bmatrix}$$

Based on the study objects, the output vector is set to be $\mathbf{y}=[\ddot{x}_s, x_g-x_u, x_u-x_s]^T$, thus the output equation is

$$\mathbf{y}=\mathbf{C}\mathbf{x}+\mathbf{H}x_g \tag{23}$$

where $\mathbf{C}=$

$$\begin{bmatrix} \frac{-k_1}{(1+\lambda_u)m_s+b} & \frac{-c_{eq}}{(1+\lambda_u)m_s+b} & \frac{k_1-\lambda_u k_2}{(1+\lambda_u)m_s+b} & \frac{c_{eq}}{(1+\lambda_u)m_s+b} \\ 1 & 0 & 0 & 0 \\ 0 & 0 & 1 & 0 \end{bmatrix}$$

$\mathbf{H}=\begin{bmatrix} \frac{\lambda_u k_2}{(1+\lambda_u)m_s+b} & 1 & 0 \end{bmatrix}^T$.

Table 2
ISO8608 values of $G_{x_g}(n_0)$.

Road level	A	B	C	D	E	F	G	H
$G_{x_g}(n_0)/(10^{-6}\mathrm{m}^{-1})$	16	64	256	1024	4096	16384	65536	262144

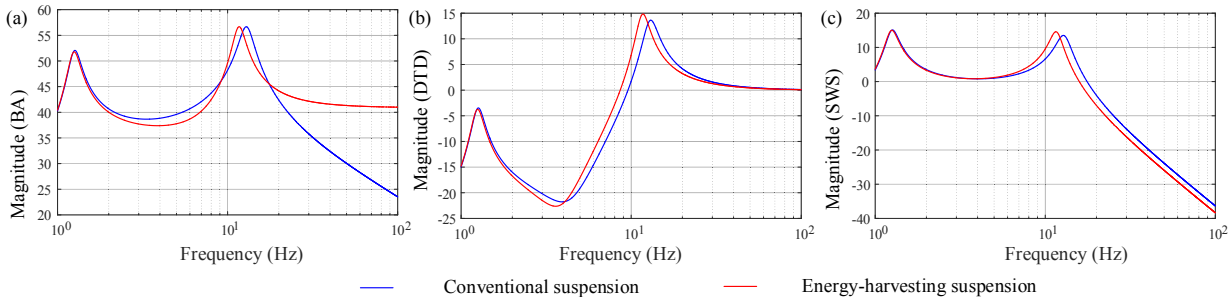

Fig. 7. The effects of inerter on the transmission characteristics (a) BA, (b) DTD, (c) SWS.

Based on the state-space Eq. (22) and output Eq. (23), the transfer functions of the system can be expressed by

$$\mathbf{G}(s)=\frac{\mathbf{Y}(s)}{\mathbf{X_g}(s)}=\mathbf{C}\left(s\mathbf{I}-\mathbf{A}\right)^{-1}\mathbf{F}+\mathbf{H} \tag{24}$$

As shown in Fig. 7, bode plots of the transfer Function (24) are used to analyze the influence of the inerter mass on energy-harvesting suspension. From Fig. 7, we can see that the ride comfort and handling stability of energy-harvesting suspension are both improved due to the contribution of the inerter in the low-frequency band (1 Hz−8 Hz for BA, 1 Hz−4 Hz for DTD), but with the sacrifice of SWS enlargement. However, the magnitude increase of SWS is so small as shown in Fig. 7 (c) that the end of the energy-harvesting damper can hardly reach the maximum stroke. Thus, the sacrifice is worthy. On the contrary, in middle frequency (8 Hz−11 Hz for BA, 4 Hz−11 Hz for DTD) the ride comfort and handling stability of energy-harvesting suspension deteriorate as a result of the effect of the inerter, whereas the SWS get better compared with the conventional suspension equipped with a hydraulic damper.

Compared with the conventional suspension, the ride comfort of an energy-harvesting suspension is improved in middle-high frequency (11 Hz−16 Hz for BA) and becomes worse in high frequency (> 16 Hz). Over 11 Hz, the handling stability (DTD) gets improved again, but the degree of improvement gradually decreases. On the contrary, the SWS get worse in such a frequency band, and the degree becomes weak with the exciting frequency.

According to ISO-8608, roads are classified into 8 levels from A to H. The road profile $x_g(x)$ is described by the power spectrum density (PSD) as:

$$G_{x_g}(n)=G_{x_g}(n_0)\left(\frac{n}{n_0}\right)^{-2} \tag{25}$$

where n is the spatial frequency (m^{-1}), n_0 is the reference spatial frequency (0.1 m^{-1}). G_0 is the road roughness coefficient, and Table 2 shows the typical values of $G_{x_g}(n_0)$ in different road levels.

When a vehicle is driving at velocity u, the temporal frequency f(Hz) can be derived from the spatial frequency n as $n = u/f$, and the power spectrum density of vertical time-varying displacement $x_g(t)$ can be obtained as

$$G_{x_g}(f)=\frac{1}{u}G_{x_g}(n) \tag{26}$$

According Eq. (26), the road power spectrum density under different road levels and different velocity of 36 km/h and 108 km/h are shown in Fig. 8. The power spectrum density decreases with the frequency exponentially, and the most road excitation frequency locates in the low frequency band ≤ 10 Hz. Compared with Fig. 7, the ride comfort is improved as a result of the inerter in such a frequency band, and the influence on SWS can be neglected. In certain excitation band of 1 Hz−4 Hz, the handling stability is also improved. These results further illustrate the feasibility of the energy-harvesting suspension.

4. The validation of the proposed regenerative variable damping suspension

4.1. Experiment test

According to Fig. 3, a scaled model experimental rig is built up to validate the properties of the proposed energy-harvesting suspension as depicted in Fig. 9. In the experiment set-up, two mounting plates that can move smoothly along the guide rods are regarded as the vehicle body and wheel, respectively, and both parts can be regulated by adding clump weights. Two springs under the bottom plate are used to imitate the tire whose damping is ignored, and the two springs between upper and bottom plates are used to imitate the suspension spring. The road input vibration is generated by a servo-electric cylinder controlled by a computer to generate different kinds of road vibration. A ball screw is connected to the generator shaft with a coupling, the generator is bolted to the upper mounting plate, and the screw-nut is connected to the bottom mounting plate. The ball screw and motor are not integrated together like some other studies, and this is because this paper focus on the control circuit and system dynamic properties, some parameters like ball screw lead, length and motor back-EMF coefficient need to be optimized in the following design of the prototype. The detailed parameters are given in Table 3. In addition, an oil damper without a moment of inerter is employed in the suspension model to be a contrast of the energy-harvesting suspension.

The road vibration x_g, the relative displacement between the vehicle body and wheel $x_s - x_u$ and displacement of the vehicle body x_s are measured by three microlaser distance sensors (HG-C1200±80 mm). In addition, the acceleration of the vehicle body is measured by an absolute acceleration sensor (ADXL203EB). All the measurement results are monitored and stored by an oscilloscope. The control part, as shown in Fig. 9, is designed according to Figs. 3 and 4. A digital signal processor based on TMS320F28035 is used to acquire and process the measurement results and generate a PWM signal to regulate the output voltage of the buck-boost converter. It also transmits the measurement results to a PC via RS485 at the same time. The circuitry for isolation between DSP and MOSFET gate is developed using a high-speed optocoupler. The phase current of the motor is measured by three Hall current sensors (HSTL-

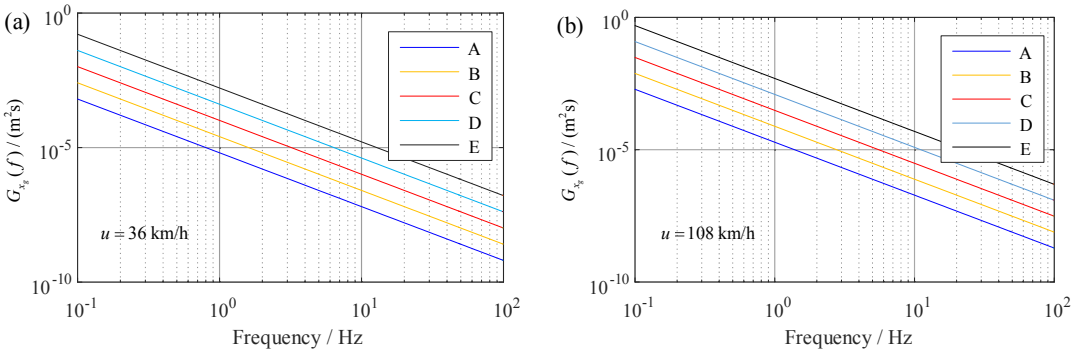

Fig. 8. Power spectrum density of road excitation under different velocities: (a) 36 km/h, (b) 108 km/h.

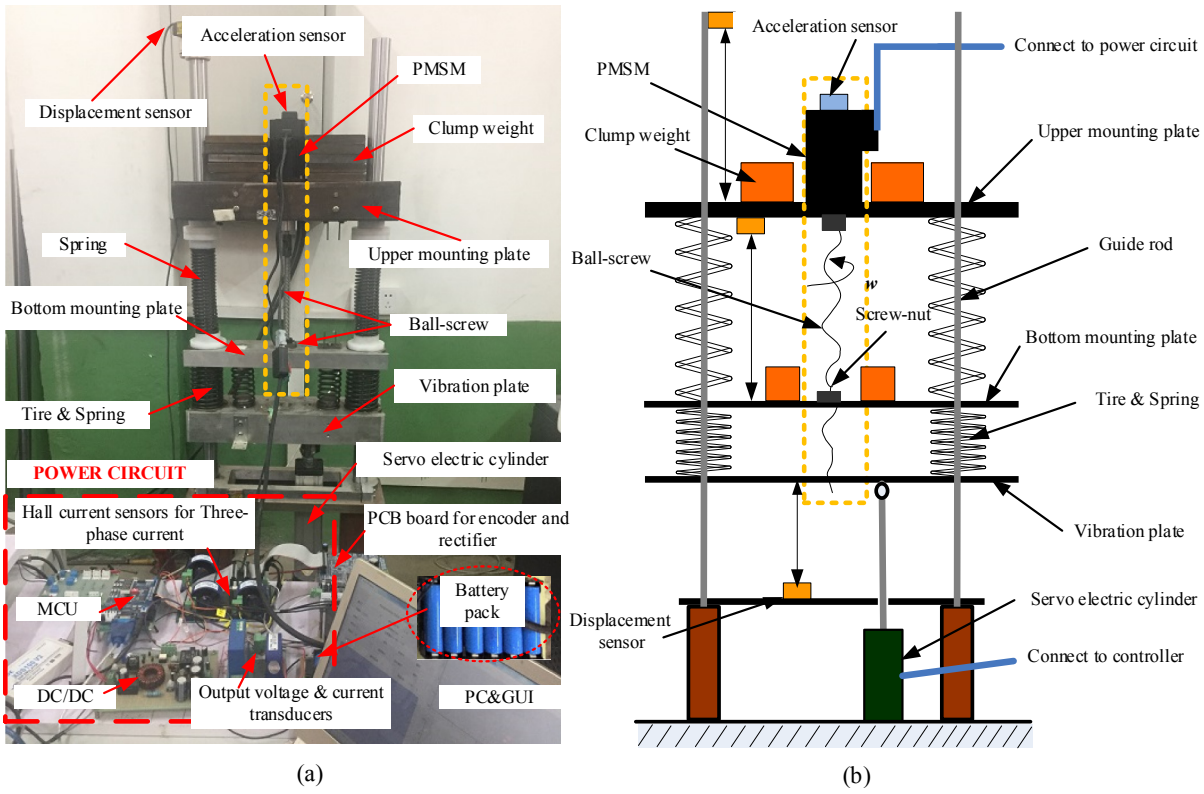

Fig. 9. A scaled experimental rig of a quarter car suspension: (a)experiment rig; (b) model of the Experiment rig.

Table 3
The parameters of the experiment set-up.

Scaled suspension parameters	Value
Sprung mass (kg)	77
Unsprung mass (kg)	7.5
Damping coefficient (Nsm^{-1})	1000
Spring stiffness (Nm^{-1})	5357
Tire stiffness (Nm^{-1})	36636
Inerter mass (kg)	7.48

in Ref. [35], the area of a force-loop means the mechanical input work ΔW of the damper in one cycle. And the equivalent damping coefficient can be calculated by

$$c_{eq} = \frac{\Delta W}{\pi \omega A^2} \tag{27}$$

where $\omega = 2\pi f$, and A is the amplitude of the sinusoid excitation. Fig. 10 shows the force-loop curves of oil damper (the nominal

Table 4
The parameters of the power circuit.

Power circuit parameters		Value
PMSM parameters	Internal Resistance (Ω)	0.7
	Inductance (mH)	12.6
	Back-EMF coefficient ($VRad^{-1}$)	0.2703
	Pole pairs	4
DC/DC converter	Inductance (mH)	76
	Capacitance (uF)	188
	Frequency (Hz)	10K
Battery package	Battery type	Li-ion
	Nominal voltage (V)	3.7
	Internal Resistance (Ω)	0.016

BLSM-300KG), and the rotor position is measured by a photoelectric encoder (2500) in the motor. The key parameters are given in Table 4.

4.2. Damping coefficient analysis

The experiment set-up can be used to measure the dynamic properties of the damper as MTS tests used in Ref. [34]. As analyzed

damping value is 1000 N/m) and electromagnetic damper (the preset value is 1000 N/m, and inerter is 7.48 kg) tested under an excitation frequency of 3 Hz and amplitudes of 3 mm, 4 mm, and 5 mm respectively. According to Eq. (27) the calculated damping results of the oil damper at three amplitudes are 1167 N/m, 1113 N/m and 930 N/m respectively, and the average is 1070 N/m. The damping values of the energy-harvesting damper at three amplitudes are 1146 N/m, 1150 N/m, 1127 N/m respectively, and the

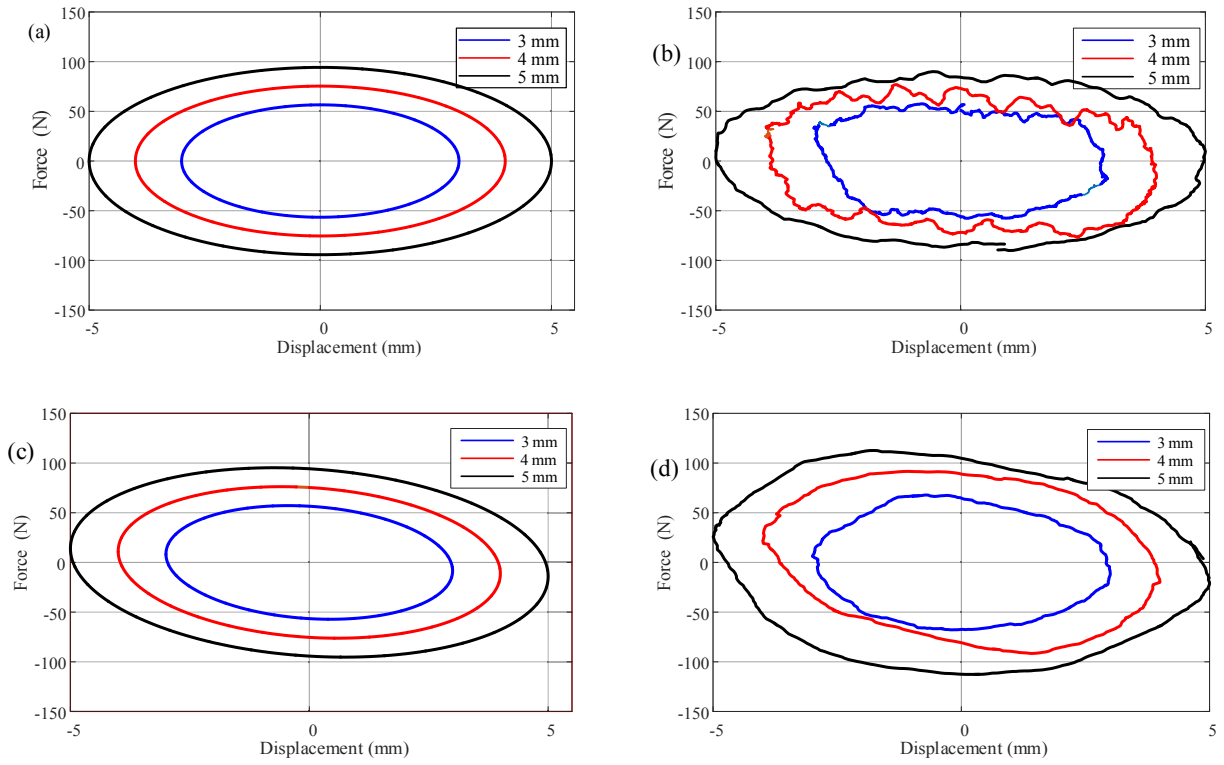

Fig. 10. Force-displacement loops results of the damper: (a) simulation results of the oil damper; (b) experiment results of the oil damper; (c) simulation results of the EMD; (d) experiment results of the EMD.

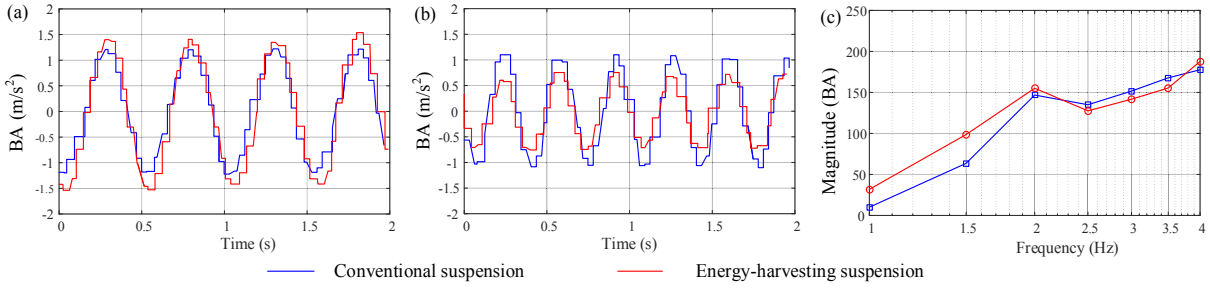

Fig. 11. The frequency and time domain responses of vehicle body acceleration (BA).

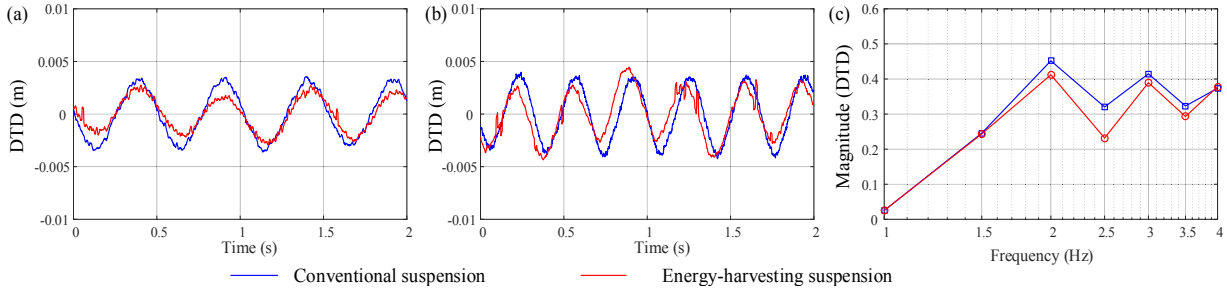

Fig. 12. The frequency and time domain response of dynamic tire deformation (DTD).

average is 1141 N/m with a 14.1% average error. This is mainly caused by the frictional resistance and viscidity resistance that comes from ball-screw and motor. As can be seen from the comparison between Fig. 10, the force-loop of the energy-harvesting damper rotates counterclockwise by a certain angle due to the effect of inerter force.

4.3. Dynamic performance comparison between energy-harvesting and conventional suspension

Under the sinusoid excitation input with an amplitude of 8 mm, the responses of $\ddot{x}_s/\dot{x}_g$, $(x_g - x_u)/\dot{x}_g$ and $(x_s - x_u)/\dot{x}_g$ in time and

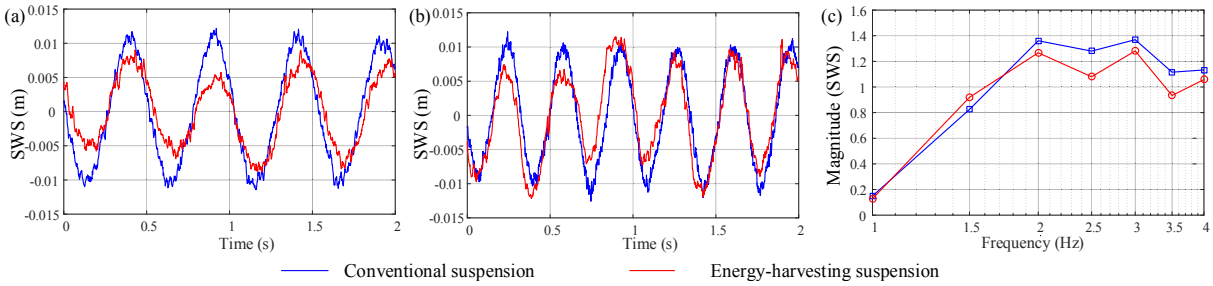

Fig. 13. The frequency and time domain response of suspension workspace state (SWS).

frequency domain are shown in Figs. 11–13, respectively. In each of the three response figures, Fig(a) and Fig(b) are the response curves in time domain under the excitation of 2 Hz and 3 Hz, and Figure (c) is the amplitude-frequency curve obtained by series of experiments.

Fig. 11 compares the acceleration responses of a conventional suspension equipped with an oil damper and an energy-harvesting suspension equipped with an EMD. It can be seen from the Fig (a) that, the ride comfort for energy-harvesting suspension gets improved a little in the middle frequency band of 2.5 Hz–3.5 Hz and gets worse in a low-frequency band below 2.5 Hz compared with the reference conventional suspension.

The energy-harvesting suspension DTD get improved in the whole frequency band of 0–4 Hz, and the SWS get improved in the high-frequency band of more than 1.7 Hz, seen from Fig (12) and Fig (13).

Combing Figs. 11–13, the energy-harvesting suspension has a very similar performance with the conventional suspension, when both have the same damping coefficient. The differences may come from the moment of inertia of the suspension, as discussed in Section 3. Further analysis of this topic will be studied in our future work.

4.4. Analysis of energy recovery capacity

For a stable system with a sinusoid excitation input, the average output power equals the average input power in a cycle when the system reaches stable compelled vibration. Thus, the system average input power can be calculated by the average power absorbed by the damper if the friction loss is neglected. The average power absorbed by damper can be obtained by

$$P_{in\_ave} = \frac{1}{T}\int_0^T P_M dt \tag{28}$$

where P_M is the instantaneous power of the generator and it is defined by $P_M = -2\pi T_{act}\Omega/60$. The minus is used to get a positive power value, because the directions of speed and torque are always opposite for a generator.

The average energy-harvesting power is obtained by the voltage and current of the battery as:

$$P_{out\_ave} = \frac{1}{T}\int_0^T i_{bat}u_{bat}dt \tag{29}$$

If friction consumption and eddy current loss in the motor is neglected, all the energy absorbed by the damper is changed into electricity, and the efficiency of the DC/DC converter can be obtained by

$$\eta_{DC/DC} = \frac{P_{out\_ave}}{P_{in\_ave}} \tag{30}$$

Considering the ball-screw mechanical transmission efficiency of 90%, the energy-harvesting efficiency is obtained by

$$\eta_{sys} = 0.90\eta_{\mathrm{DC/DC}} \tag{31}$$

Tested with an excitation input characterized with the amplitude of 8 mm and frequency of 2 Hz, Fig. 14 (a) shows the curves of speed and torque with time, and Fig. 14 (b) shows the curve of instantaneous input power with time. The direction of motor torque and speed values are always opposite, which illustrates that the motor works in generator mode. Fig. 15 (a) shows the curves of battery voltage and current with time, and (b) shows the curve of

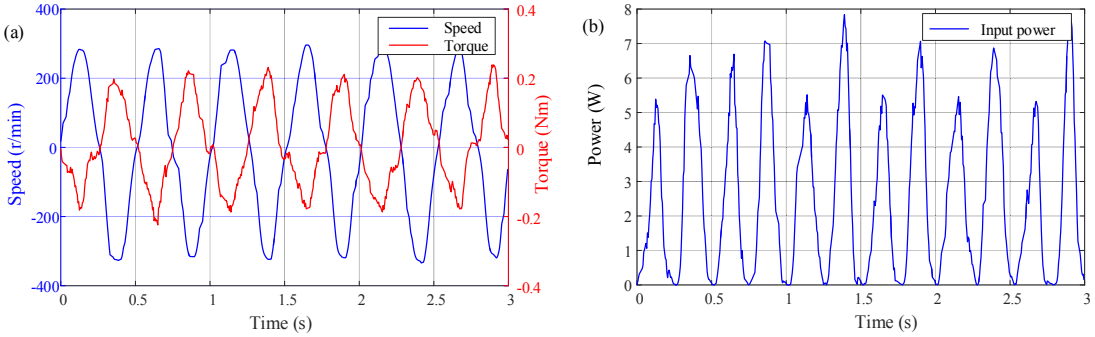

Fig. 14. System instantaneous input power evaluated based on the energy absorbed by the damper: (a) the curves of speed and torque with time; (b) the curve of instantaneous input power with time.

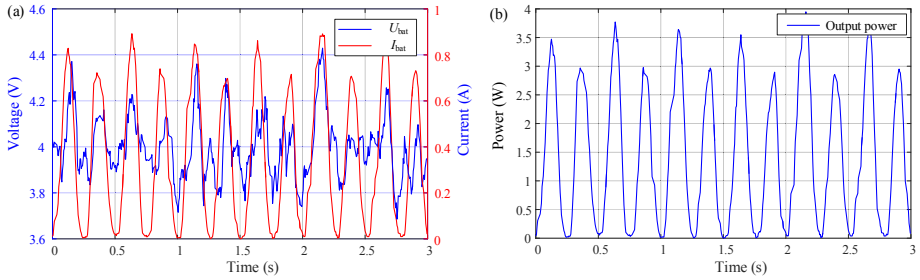

Fig. 15. System instantaneous output power evaluated based on the energy absorbed by the battery: (a) the curves of voltage and current with time; (b) the curve of instantaneous output power with time.

Table 5
Average input and output power tested in c_{eq_ref}=1000 N/m, A = 8 mm, T = 3s.

Power & Efficiency	Frequency			
	1.5 Hz	2 Hz	3 Hz	4 Hz
Average input power P_{in_ave} (W)	1.61	2.17	3.66	4.02
Average output power P_{out_ave} (W)	1.16	1.25	2.62	3.36
DC/DC Efficiency $\eta_{DC/DC}$ (%)	72.32	57.57	71.43	83.60
System energy-harvesting efficiency η_{sys} (%)	65.09	51.81	64.29	75.24

instantaneous output power with time. The battery voltage varied with the current as a result of battery inner resistance.

Table 5 lists the average input power according to Eq. (28), average output power according to Eq. (29), the average efficiency of DC/DC converter according to Eq. (30) and energy-harvesting efficiency of the system according to Eq. (31) from excitation frequency of 1.5 Hz–4 Hz. The results show that the higher the excitation frequency, the greater the average input and output power. The DC/DC converter efficiency and system energy-harvesting efficiency vary in a wide range with the excitation frequency, the minimum and maximum efficiencies are 51.81% and 75.24% respectively. Comparing to Refs. [21,29], where the average efficiencies are about 40% and 44.24%, the efficiency of this proposed methods has improved by 11.81%–35.24% and 7.57%–31% respectively.

5. Conclusions

To simultaneously harvest/storage the vibration energy and control the damping of the suspension, the energy-harvesting variable/constant damping suspension system with motor based electromagnetic damper has been proposed in this paper. The design and realization of the energy-recovery damping variable suspension was firstly proposed in system level. The proposed energy-harvesting variable/constant damping suspension system was then modeled and analysis. How the moment of inertia composed from the motor rotor and transmission affects the performance of a suspension was evaluated. Simulations and experiments with a 2DOF suspension model were conducted to verify the proposed energy-harvesting suspension. It was shown from the results that small moment of inertia of the EMD as the proposed system can both improve the ride comfort and handle stability of the suspension, which illustrated the feasibility of the energy-harvesting suspension. The proposed damping closed-loop control circuit can ensure the damping coefficient a preset constant value with an error of 14.1% while harvesting energy from the vibration. And the energy-harvesting efficiency was as high as 51.81%–75.24%, with as high as 35.24% improvement.

This paper introduced a solution of design and realization of an energy-harvesting damping variable suspension system in detail. Both the energy harvest and damping control are realized simultaneously. The energy can not only be harvested, but also be stored for further usage. Meanwhile, the damping of the suspension system can be controlled as wish, both be variable and constant. The study of this paper can be a good guidance for future studies of the energy-harvesting suspension.

Acknowledgments

The authors are grateful for the financial support from the Ministry of Industry and Information Technology Green Manufacturing System Integration Project, Shaanxi Key Research and Development Plan Industry Innovation Chain Project (2019ZDLGY15-04-01), the National Natural Science Foundation of China under Grant 51405374and the Fundamental Research Funds for the Central Universities (xjj2018043).

References

[1] Suri G, Onori S. A control-oriented cycle-life model for hybrid electric vehicle lithium-ion batteries. Energy 2016;96:644–53.
[2] Cai Y, Yang L, Deng Z, Zhao X, Deng H. Online identification of lithium-ion battery state-of-health based on fast wavelet transform and cross D-Markov machine. Energy 2018;147:621–35.
[3] Wang B, Xu J, Cao B, Zhou X. A novel multimode hybrid energy storage system and its energy management strategy for electric vehicles. J Power Sources 2015;281(0):432–43.
[4] Li Y, Xu J, Mei X, Wang J. A unitized multiwinding transformer based equalization method for series-connected battery strings. IEEE Trans Power Electron 2019. https://doi.org/10.1109/TPEL.2019.2910205.
[5] Xu J, Cao B, Wang J. A novel method to balance and reconfigure series-connected battery strings. Energies 2016;9(10):766.
[6] Zhang H, Zhu C, Zheng W, You S, Ye T, Xue P. Experimental and numerical investigation of braking energy on thermal environment of underground subway station in China's northern severe cold regions. Energy 2016;116:880–93.
[7] Qiu C, Wang G, Meng M, Shen Y. A novel control strategy of regenerative braking system for electric vehicles under safety critical driving situations. Energy 2018;149:329–40.
[8] Abdelkareem MAA, Xu L, Ali MKA, El-Daly A-RBM, Hassan MA, Elagouz A, Bo Y. Analysis of the prospective vibrational energy harvesting of heavy-duty truck suspensions: a simulation approach. Energy 2019;173:332–51.
[9] Julien C, Mauger A, Vijh A, Zaghib K. Lithium batteries. In: Lithium batteries. Springer International Publishing; 2016. p. 29–68.
[10] Zuo L, Zhang P-S. Energy harvesting, ride comfort, and road handling of regenerative vehicle suspensions. J Vib Acoust 2013;135(1):011002.
[11] Zhang Y, Guo K, Wang D, Chen C, Li X. Energy conversion mechanism and regenerative potential of vehicle suspensions. Energy 2017;119:961–70.
[12] Wei C, Taghavifar H. A novel approach to energy harvesting from vehicle suspension system: half-vehicle model. Energy 2017;134:279–88.
[13] Gao Z, Chen S, Zhao Y, Liu Z. Numerical evaluation of compatibility between comfort and energy recovery based on energy flow mechanism inside electromagnetic active suspension. Energy 2019;170:521–36.
[14] Zhang Y, Zhang X, Zhan M, Guo K, Zhao F, Liu Z. Study on a novel hydraulic pumping regenerative suspension for vehicles. J Frankl Inst 2015;352(2):485–99.
[15] Karnopp D. Permanent magnet linear motors used as variable mechanical dampers for vehicle suspensions. Veh Syst Dyn 1989;18(4):187–200.
[16] Duong MT, Chun YD, Hong DK. Design of a high-performance 16-slot 8-Pole electromagnetic shock absorber using a novel permanent magnet structure.

Energies 2018;11(12).
[17] Ebrahimi B, Bolandhemmat H, Khamesee MB, Golnaraghi F. A hybrid electromagnetic shock absorber for active vehicle suspension systems. Veh Syst Dyn 2011;49(1–2):311–32.
[18] Asadi E, Ribeiro R, Khamesee MB, Khajepour A. Analysis, prototyping and experimental characterization of an adaptive hybrid-electromagnetic damper for automotive suspension systems. IEEE Trans Veh Technol 2016;PP(99). 1-1.
[19] Li S, Xu J, Pu X, Tao T, Mei X. A novel design of a damping failure free energy-harvesting shock absorber system. Mech Syst Signal Process 2019;132:640–53.
[20] Zhang G, Cao J, Yu F. Design of active and energy-regenerative controllers for DC-motor-based suspension. Mechatronics 2012;22(8):1124–34.
[21] Salman W, Qi L, Zhu X, Pan H, Zhang X, Bano S, Zhang Z, Yuan Y. A high-efficiency energy regenerative shock absorber using helical gears for powering low-wattage electrical device of electric vehicles. Energy 2018;159:361–72.
[22] Guo S, Xu L, Liu Y, Guo X, Zuo L. Modeling and experiments of a hydraulic electromagnetic energy-harvesting shock absorber. IEEE ASME Trans Mechatron 2017;22(6):2684–94.
[23] Sabzehgar R, Maravandi A, Moallem M. Energy regenerative suspension using an algebraic screw linkage mechanism. IEEE ASME Trans Mechatron 2014;19(4):1251–9.
[24] Pires L, Smith MC, Houghton NE, McMahon RA. Design trade-offs for energy regeneration and control in vehicle suspensions. Int J Control 2013;86(11):2022–34.
[25] Zhang Y, Chen H, Guo K, Zhang X, Eben Li S. Electro-hydraulic damper for energy harvesting suspension: modeling, prototyping and experimental validation. Appl Energy 2017;199:1–12.
[26] Ning D, Sun S, Du H, Li W, Zhang N. Vibration control of an energy regenerative seat suspension with variable external resistance. Mech Syst Signal Process 2018;106:94–113.
[27] Chen SA, Li X, Zhao LJ, Wang YX, Kim YB. Development of a control method for an electromagnetic semi-active suspension reclaiming energy with varying charge voltage in steps. Int J Automot Technol 2015;16(5):765–73.
[28] Okada Y, Harada H. Regenerative control of active vibration damper and suspension systems. In: Proceedings of 35th IEEE conference on decision and control. vol. 4; 1996. p. 4715–20. vol. 4.
[29] Zhang Z, Zhang X, Chen W, Rasim Y, Salman W, Pan H, Yuan Y, Wang C. A high-efficiency energy regenerative shock absorber using supercapacitors for renewable energy applications in range extended electric vehicle. Appl Energy 2016;178:177–88.
[30] Wang R, Ding R, Chen L. Application of hybrid electromagnetic suspension in vibration energy regeneration and active control. J Vib Control 2016;24(1):223–33.
[31] Guo S, Liu Y, Xu L, Guo X, Zuo L. Performance evaluation and parameter sensitivity of energy-harvesting shock absorbers on different vehicles. Veh Syst Dyn 2016;54(7):918–42.
[32] Lee JG, Park CS, Lee JJ, Cho HI, Hong JP, Lee GH. Characteristic analysis of brushless motor considering drive type. Seoul (Korea): The Korean Institute of Electrical Engineers; 2002. p. 589–91. Medium: X; Size: page(s).
[33] Lefeuvre E, Audigier D, Richard C, Guyomar D. Buck-boost converter for sensorless power optimization of piezoelectric energy harvester. IEEE Trans Power Electron 2007;22(5):2018–25.
[34] Xie L, Li J, Cai S, Li X. Electromagnetic energy-harvesting damper with multiple independently controlled transducers: on-demand damping and optimal energy regeneration. IEEE ASME Trans Mechatron 2017;22(6):2705–13.
[35] Li Z, Zuo L, Luhrs G, Lin L, Qin Yx. Electromagnetic energy-harvesting shock absorbers: design, modeling, and road tests. IEEE Trans Veh Technol 2013;62(3):1065–74.